The Motion and Wake Characteristics of Bottom Blowing Coaxial Double Bubbles

Yutang Zhao[a, b], Xiaohui Zhang[a,b, *], Xinting Tong[c], Xiaolv Yu[c], Jing Luo[c], Yanxiong Fu[c], Hua Wang[a,b]

[a]Faculty of Metallurgical and Energy Engineering, Kunming University of Science and Technology, Kunming 650093, China

[b]National local Joint Engineering Research Center of Energy Saving and Environmental Protection Technology in Metallurgy and Chemical Engineering Industry, Kunming University of Science and Technology, Kunming 650093, China

[c]Yimen COPPER Corp. Ltd. 650093, Yimen 651100, China

[*] Corresponding author. E-mail address: xiaohui.zhang@kust.edu.cn

Abstract *: In the process of bottom blowing bath smelting, continuous bubbles are formed and rise in the melt after the bottom blowing gas is ejected. In order to reveal the motion behavior and wake characteristics of continuous bubbles formed during the injection process, the rising process of coaxial double bubbles is studied through numerical simulation, the velocity and deformation characteristics of coaxial double bubbles in the rising process are obtained. Based on the vortex identification reconstruction of the flow field, the characteristics of formation, evolution, and configuration of bubble wake are obtained. The results show that in terms of motion characteristics, the aspect ratio of the upper bubble is always less than 1, and lower bubble has a large span of change: The minimum is 0.85 and the maximum is 1.2. As the two bubbles approach, the aspect ratio of the upper bubble is always less than 1, while the maximum aspect ratio of the lower bubble can reach 1.2. In terms of wake characteristics, the vorticity on the upper bubble surface is larger. When the wake rotation centers of the upper and lower bubbles merge with each other, the instantaneous acceleration of the lower bubble reaches the maximum.*

Key words *: Bath smelting, Bubble motion behavior, Wake, Numerical simulation, Vortex identification*

1 Introduction

The phenomenon of bubble motion in liquid is widely found in metallurgy and chemical industry. In multiphase flow systems, the generation, motion, and interaction of bubbles all have important effects on the gas-liquid phase [1-4]. In the process of bottom blowing bath smelting, gas enters the melt through the spray gun and disperses in the form of bubbles, thereby affecting the mixing time of gas and liquid [5]. The bubble rising behavior can affect the melt flow and

heat and mass transfer process, which has an important influence on the smelting process. Revealing the bubble movement behavior can provide an important theoretical basis for the actual production process and equipment optimization [6-9].

According to the initial state, the research on multi-bubbles is mainly divided into two types : parallel and vertical (coaxial). In terms of the motion characteristics of parallel multi-bubbles, Dekée [10] and Liu [11] studied the effects of initial bubble diameter, initial horizontal spacing and rheological properties of non-Newtonian fluid on the interaction between bubbles for the coalescence of two and three bubbles in Newtonian and non-Newtonian fluid. Kong et al. [12] studied the interaction between parallel double bubbles during the rising process and proposed a function of the interaction force and liquid viscosity. The results showed that bubble deformation plays an important role in bubble interaction and path instability.

Regarding the interaction between coaxial multi bubbles, some scholars [13-16] have shown that the interaction between bubbles can significantly affect the trend of bubble collision and coalescence, and the deformation of bubbles affects the interaction between bubbles. Narayanan et al. [17] studied the coalescence characteristics of five different types of bubbles and established equations for predicting the velocities of upper (u_1) and lower (u_2) bubbles in coalescence process. Li et al. [18] analyzed the evolution of bubble coalescence process by studying the formation and coalescence process of coaxial double bubbles, and according to their research, the phase diagrams of coaxial bubble coalescence and non-coalescence are established based on *We* number and *Mo* number.

In addition to the study of bubble motion behavior characteristics, a considerable portion of research has also focused on the wake characteristics of bubbles. Komasawa et al. [19] studied the dynamic behavior of a single and a pair of spherical cap shaped bubbles at rest in a liquid flow field flowing vertically downwards, and proposed three types of bubble wake: flaky wake (or laminar wake, $Re = 10 \sim 90$), transitional wake ($Re = 90 \sim 500$) and turbulent wake ($Re > 500$). Cano Lozano et al. [20, 21] studied the trajectory and wake of bubbles with numerical simulation, and their research results indicate that the unstable rise of bubbles is caused by asymmetric shedding of the bubble wake. Zhang et al. [22] showed that the symmetry of the vortex structure in the bubble wake is destroyed, causing the upward trajectory of the bubble to change from the zigzag shape to the spiral shape.

The motion of bubbles has characteristics such as nonlinearity, instability, and non-uniformity, and their interphase interactions are complex and variable, which have significant impacts on industrial processes such as chemical and metallurgical industries [23-25]. In the process of bottom blown molten pool melting, due to the large distance between the bottom blown spray guns, the interaction between parallel multiple bubbles is weaker than that of vertical multiple bubbles [26-29]. Therefore, this paper focuses on the study of the upward motion behavior and wake characteristics of vertical double bubbles. In terms of motion characteristics, the influence of initial bubble spacing and diameter is investigated. In terms of wake characteristics, the Ω vortex identification method is used to study the configuration and strength change of double bubbles wake.

2 Model establishment and validation

2.1 Physical model.

Considering that the rising process of bubbles is not affected by the wall, the distance between the bubble and the side wall is at least greater than 6 times the bubble diameter, and the model height should be high enough to make the bubble change process complete enough. Therefore, a two-dimensional rectangular calculation domain of 0.2 m × 0.5 m is constructed. In the two-dimensional computational domain, the two bubbles are circular and have the same initial diameter. The initial position of the lower bubble (B2) is located at the center of the x-axis, 10mm from the bottom of the model, and the initial position of the upper bubble (B1) is directly above the lower bubble. As shown in Fig.1 (a), the shortest distance between the upper and lower bubble boundaries is *s*. ICEM is a pre-processing software for fluid simulation, and it is mainly used for the physical modeling and grid generation. In order to improve the simulation accuracy and not to increase the calculation load as much as possible, the local grid refinement is carried out in the bubble rising area, and the refinement area is 0.04m × 0.5m, as shown in Fig.1 (b).

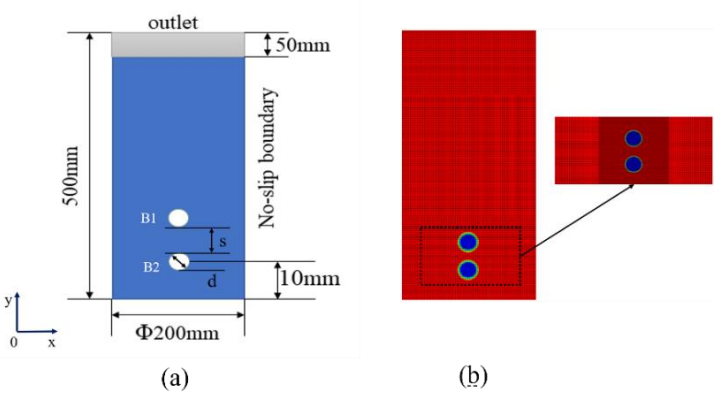

Fig. 1 Physical model and grid

2.2 Mathematical model

(1) Multiphase flow model

Volume of Fluid (VOF) model is mainly used to solve the problem of two-phase flow with clear interface. For the gas-liquid two-phase, the tracking of the interface between the phases in the VOF model is completed by solving the continuity equation of the volume fraction. The continuity equation of the q phase is:

$$\frac{\partial \alpha_q}{\partial t} + V_q \cdot \nabla \alpha_q = \frac{S_{\alpha q}}{\rho_q} + \frac{1}{\rho_q}\sum_{q=1}^{n} m_{pq} - m_{qp} \tag{1}$$

In the formula: ρ_q is the density of q phase; α_q is the volume fraction of q phase; V_q is the velocity of q phase; m_{pq} is the mass transport of q phase and p phase in the fluid; $S_{\alpha q}$ is the source term.

In the VOF model, a momentum equation is solved in the whole region, and the obtained velocity field is shared between the phases. The momentum equation is as follows:

$$\frac{\partial}{\partial t}(\rho\vec{V}) + \nabla \cdot (\rho\vec{V}\vec{V}) = -\nabla p + \nabla \cdot \left[\mu(\nabla\vec{V} + \nabla\vec{V}^T)\right] + \rho\vec{g} + \vec{F} \tag{2}$$

Among them, $\vec{F}$ is the volume force acting on the control volume, N.

(2) Turbulence model

The standard k-ε model can determine two turbulence lengths and time scales by solving two independent transport equations, which is applicable to both gas and liquid and has wide applicability. The turbulence model used in this study is the Standard *k-ε* model, where *k* and *ε* represent turbulent kinetic energy and turbulent dissipation rate, respectively. The equations are as follows:

$$\frac{\partial}{\partial t}(\rho k)+\frac{\partial}{\partial x_j}(\rho k u_j)=\frac{\partial}{\partial x_j}\left[\mu+\frac{\mu_t}{\sigma_k}\frac{\partial k}{\partial x_j}\right]+G_k+G_b-\rho\varepsilon+S_k \quad (3)$$

$$\frac{\partial}{\partial t}(\rho \varepsilon)+\frac{\partial}{\partial x_j}(\rho \varepsilon u_j)=\frac{\partial}{\partial x_j}\left[\left(\mu+\frac{\mu_t}{\sigma_\varepsilon}\right)\frac{\partial \varepsilon}{\partial x_j}\right]+\rho C_1 S_\varepsilon-\rho C_2\frac{\varepsilon^2}{k+\sqrt{v\varepsilon}}+C_{1\varepsilon}\frac{\varepsilon}{k}C_{3\varepsilon}G_b+S_\varepsilon \quad (4)$$

Among them，

$$C_1=max\left[0.43,\frac{\eta}{\eta+5}\right],\eta=S\frac{k}{\varepsilon},S=\sqrt{2S_{ij}S_{ij}},S_{ij}=\frac{1}{2}\left(\frac{\partial u_j}{\partial x_i}+\frac{\partial u_i}{\partial x_j}\right)$$

G_k is the average velocity gradient; G_b is the turbulent kinetic energy generated by buoyancy; C_2、$C_{1\varepsilon}$ and $C_{3\varepsilon}$ are constants; σ_k and σ_ε are the Turbulent Prandtl numbers of *k* and *ε*; S_k and S_ε are user-defined source terms; *S* is the scalar measure of the deformation tensor; S_{ij} is the average strain rate.

2.3 Vortex identification method

Liu et al. proposed the *Ω* vortex identification method, which is based on the Helmholtz velocity decomposition principle. The vorticity is further decomposed into a rotating part and a non-rotating part. The physical meaning is the ratio of the rotational vorticity to the total vorticity, which is expressed as:

$$\Omega=\frac{\|B\|_F^2}{\|A\|_F^2+\|B\|_F^2+a} \quad (5)$$

Among them，$'a'$ is a variable related to the dimension of the computational domain. The approximate expression of $'a'$ is [30]:

$$a=0.002Q\left((\|B\|_F^2-\|A\|_F^2)\right)_{max_{max}} \quad (6)$$

In the above equation, $\|\boldsymbol{B}\|_{\boldsymbol{F}}$ represents the Frobenius norm of matrix ***B***. Matrix ***A*** is composed of linear deformation rate and angular deformation rate while matrix ***B*** is composed of rotational angular velocity, so ***A*** is called symmetric tensor and ***B*** is called antisymmetric tensor. According to equation (4), the value range of *Ω* is $0 \le \Omega \le 1$, which can be understood as the concentration of vorticity, representing the rigidity of fluid motion. When *Ω*=1, it represents the fluid rotating as a rigid body. When *Ω*>0.5, it indicates that the proportion of antisymmetric tensor ***B*** is superior to symmetric tensor ***A***. Therefore, *Ω* slightly greater than 0.5 is used as the criterion for vortex identification. In this paper, we choose liu [30] ' s suggestion to use *Ω* = 0.52 as the threshold to judge the vortex boundary.

2.4 Computational setup and grid independence validation

The outlet is set as a pressure outlet, the solid wall is set as a non-slip boundary, the standard wall functions is used for processing within the wall boundary layer; The time step is

1×10^{-4}s.

To ensure the accuracy of the calculation, grid independence testing is required. The initial bubble diameter d=6mm and the initial bubble spacing s=12mm. Performing the independence verification on grids of 26000(A), 250000(B), 630000(C), 810000(D), and 1.28 million(E), respectively.

Fig. 2 shows the positions and heights of bubbles B1 and B2 at different times. It can be seen from the figure that the bubble motion heights of grids C, D and E basically do not change with the number of grids. Therefore, in order to save computing resources, grid C is selected for calculation.

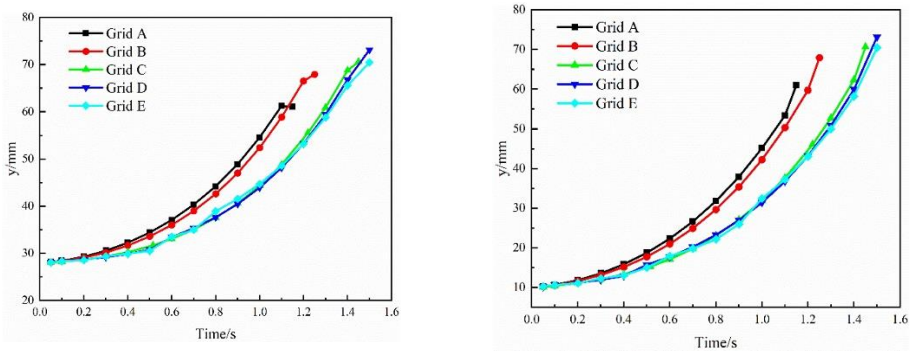

(a) Height variation of upper bubble (B1) (b) Height variation of lower bubble (B2)

Fig.2 Position of bubble under different grid numbers.

2.5 Validation of coaxial twin-bubble model

Tian et al. [15] conducted experimental studies on the upward motion of coaxial double bubbles of different sizes in high viscosity fluids. In order to validate the mathematical model constructed in this paper, calculation conditions are set according to the experimental conditions in reference [15] (as shown in Table 1). The physical model used in the verification is a two-dimensional structure. The size of the model, the basic physical parameters of bubbles and liquids, and the simulation conditions are consistent with the reference 13. The rising process of bubbles is simulated. The shape of the double bubble rise process at different times is compared with the experiment, as shown in Fig. 3.

Table 1 Experimental conditions of Tian et al. [15]

	T/K	**ρ/(kg/m^3)**	**μ/(Pa·s)**	**σ/(n/m)**	**d/mm**
case	293	970	0.3003	0.0203	6

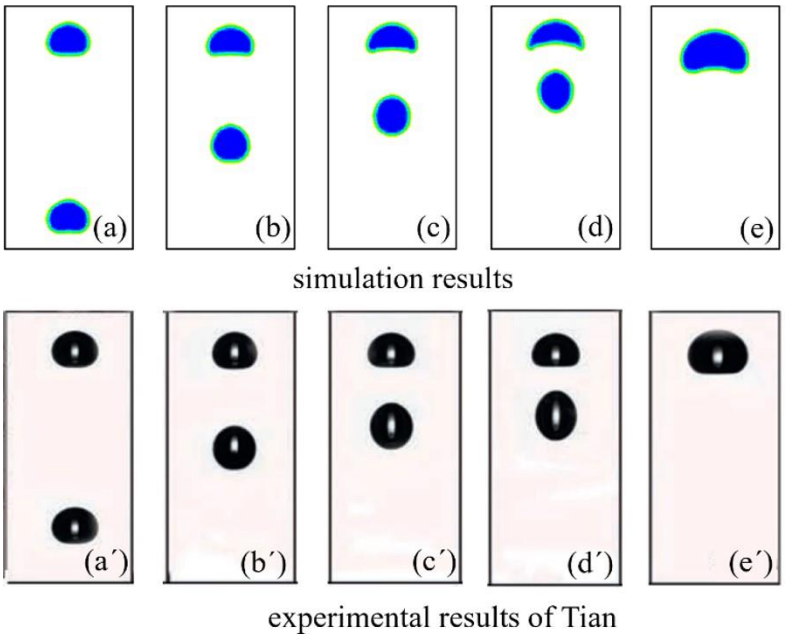

Fig.3 The comparison of bubbles rising process between simulation and experiment

From the comparison of experimental and numerical simulation results in Fig. 3, it can be seen that the position changes during the rising process and the shape changes during the continuous approaching process are highly consistent. Therefore, it can be considered that the model established in this study is reliable.

2.6 Simulation Conditions

In this paper, the rising process of coaxial double bubbles (physical property is air) with the same initial diameter in oil ($1261\rho/(kg/m^3)$, $0.00869\mu/(Pa \cdot s)$, $0.021\sigma/(N/m)$) is studied. The diameters (d) of the double bubbles are 4mm, 6mm and 8mm, respectively (referring to the experiment of Tian et al.). The initial bubble spacing s are $0.5d$, $1d$, $1.5d$, $2d$, $3d$ and $4d$ respectively. The simulation conditions are shown in Table 2. The comparative simulation conditions are: the single bubble rising process with the same position as the lower bubble (B2) and the diameter of 4mm, 6mm and 8mm respectively.

Tab.2 Calculation conditions

Category	Initial bubble spacing					
4mm	0.5d	1d	1.5d	2d	3d	4d
6mm	0.5d	1d	1.5d	2d	3d	4d
8mm	0.5d	1d	1.5d	2d	3d	4d

3 Results and Discussion

In this study, the effects of different initial spacing and bubble diameter on the motion characteristics and wake characteristics of double bubbles are analyzed from the aspects of instantaneous velocity of bubbles, velocity vector of liquid phase, bubble shape change, bubble aspect ratio (E), and formation and intensity of bubble wake. Due to the large relative surface tension of the gas and liquid in this study, the small size of the model, the height of the bottom

of the liquid surface, etc., the rising trajectory of the bubble is stable, showing a straight rise phenomenon, the coaxial double bubbles on the straight line are approximately analyzed.

3.1 Velocity Characteristics

3.1.1 Bubble Velocity Characteristics

The bubble centroid is selected as the reference point of the instantaneous velocity of the bubble. Fig. 4 is the instantaneous velocity of the bubbles during the rising process with diameters of 4mm, 6mm and 8mm, respectively. It can be seen from the figure that in the initial stage, the two bubbles rise relatively independently. As the two bubbles approach, the instantaneous velocity of the lower bubble suddenly decreases. As the two bubbles merge, the instantaneous velocity of the upper and lower bubble are the same. This is because the upper surface of the upper bubble is subjected to liquid resistance during the rising process, and the lower surface is subjected to liquid viscous force, so that the liquid below the upper bubble forms an upward velocity field. According to the continuity of the fluid, the lower bubble will also be affected by the velocity field, that is, the lower bubble is affected by the wake suction of the upper bubble, so that the velocity of the lower bubble is greater than that of the upper bubble, which also causes the lower bubble to rise rapidly near the upper bubble and coalesce. As the initial spacing increases, the longer the time required for bubble coalescence, the greater the distance of independent rise, and the greater the speed of coalescence. As the bubble diameter increases, the shorter the time required for coalescence, the greater the speed of coalescence. The acceleration of the coaxial double bubble rising process is much larger than that of the single bubble, and the larger the initial distance and the larger the bubble radius, the greater the difference between the acceleration of the coaxial double bubbles and the single bubble.

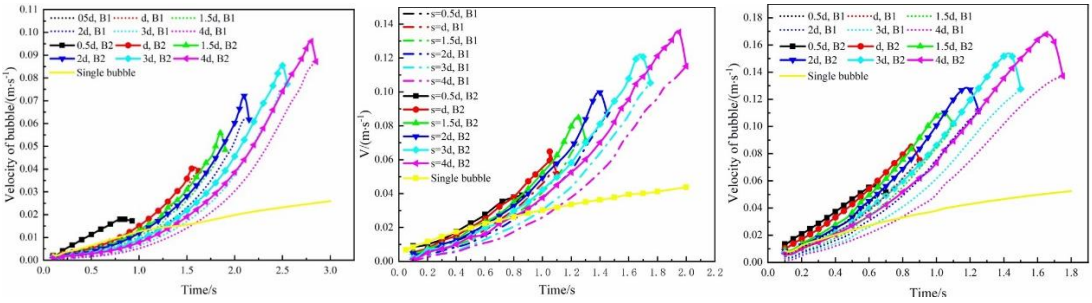

(a) 4mm (b) 6mm (c) 8mm

Fig.4 Instantaneous speed change of B1 and B2

3.1.2 Liquid Phase Velocity Vector

Figs.5-7 show the velocity vector distribution of the rising process of coaxial double bubbles with different diameters when the initial spacing $s = 2d$. The direction of the arrow represents the direction of fluid motion, the length of the line represents the magnitude of the speed. L is the relative distance between two bubbles that are constantly approaching，that is L = bubble spacing/initial bubble spacing. It can be seen from Figs.5-7 that the bubble will disturb the surrounding fluid during the rising process, so that the surrounding fluid forms a regular flow field. As L continues to decrease, the velocity vector becomes denser and the flow field distribution becomes more complex. And then, it can be seen from the density of the vector line

that the influence of the double bubbles with a diameter of 4mm on the fluid is lower than that of 6mm and 8mm, that is, the larger the initial diameter, the greater the influence of the double bubbles on the flow field. Since the vector distribution trends shown in Figs. 5-7 are consistent, only Fig. 5 is analyzed here.

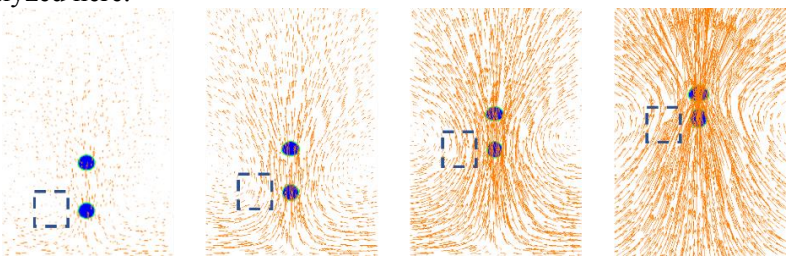

(a) L=1.75d (b)L=1.25d (c)L=0.75d (d)L=0.25d

Fig.5 Double bubble velocity vector diagram with diameter of 4mm

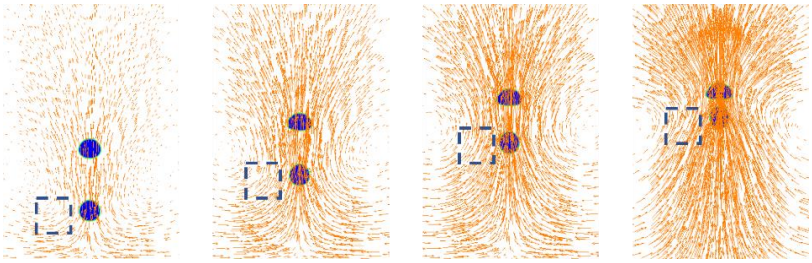

(a) L=1.75d (b)L=1.25d (c)L=0.75d (d)L=0.25d

Fig.6 Double bubble velocity vector diagram with diameter of 6mm

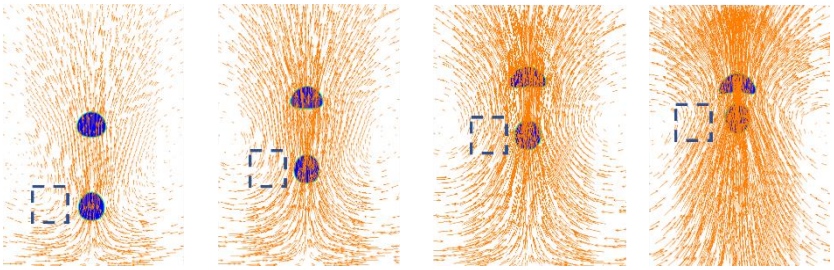

(a) L=1.75d (b)L=1.25d (c)L=0.75d (d)L=0.25d

Fig.7 Double bubble velocity vector diagram with diameter of 8mm

It can be seen from Fig.5 that the velocity direction of the left and right sides of the upper bubble deflects. There are two counter-rotating vortexes (the wake of the upper bubble) symmetrically distributed on the upper side of the lower bubble, that is, the lower side of the upper bubble. From the direction of the vector line in the diagram, it can be seen that the left vortex is counterclockwise and the right side is clockwise, forming two symmetrical vortex circulation flows. The direction of the lower boundary vector of the vortex is consistent with the direction of the lower bubble motion, which promotes the acceleration of the lower bubble. The vortex structure of the blue frame line in the figure is analyzed. When L = 1.75d, the vortex is weak and has little effect on the lower bubble. The vortex is distributed above the lower bubble side. When L = 1.25d and L = 0.75d, the vortex position decreases, and the driving effect on the lower bubble is strengthened, which promotes the coalescence of double bubbles. When L = 0.25d, the two bubbles are about to coalesce. At this time, the lower bubble is already above the symmetrical vortex structure. The symmetrical vortex forms an upward velocity to push the

bubble up, further promoting the lower bubble to accelerate close to the upper bubble.

3.2 Bubble Deformation Characteristics

The bubble aspect ratio (E) is used as a quantitative index to describe the deformation characteristics of the bubble. The aspect ratio (E) of a bubble is the ratio of its longitudinal diameter to its transverse diameter. The more the aspect ratio (E) deviates from 1, the more serious the deformation of the bubble is. As shown in 8, the aspect ratio of the bubble $E = d\,2 / d\,1$.

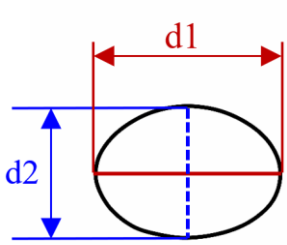

Fig. 8 Schematic diagram of bubble aspect ratio

Fig.9 shows the aspect ratio of coaxial double bubbles with diameters of 4mm, 6mm and 8mm. When the initial spacing s is different, the aspect ratio E of upper and lower bubble changes. With the increase of the initial spacing, the mutual ability between two bubbles are weakened, and the change range of aspect ratio of the two bubbles is reduced, and both are close to the aspect ratio curve of the single bubble. Since the initial placement height of the lower bubble is consistent with that of the single bubble, the larger the initial spacing is, the closer the aspect ratio change trend of the lower bubble is to that of the single bubble. The larger the initial spacing, that is, the higher the placement height of the upper bubble, the smaller the aspect ratio change range of the upper bubble. This is because the amount of liquid in the upper part of the upper bubble decreases, and the liquid pressure on the bubble is reduced, resulting in a more stable bubble shape and a slow change of the aspect ratio. Under different initial spacing, the aspect ratio of the lower bubble with a diameter of 4mm changes between 0.9 and 1.1, the aspect ratio of the lower bubble with a diameter of 6mm is between 0.9 and 1.2, and the aspect ratio of the lower bubble with a diameter of 8mm is between 0.85 and 1.25. The smaller the diameter, the more stable the shape.

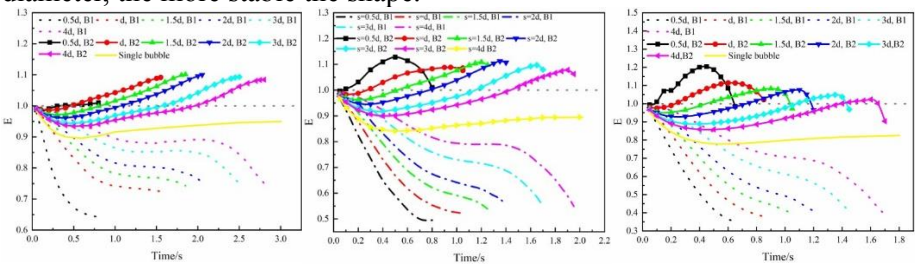

（a）d=4mm (b) d=6mm (c) d=8mm

Fig.9 Deformation of double bubbles with different diameters

The variation pattern of the aspect ratio of coaxial double bubbles with diameters of 4mm, 6mm, and 8mm is consistent according to Fig. 9, only the shape changes of coaxial double bubbles with d=6mm and s=2d were analyzed, as shown in Fig. 10, which shows the shape changes of upper and lower bubbles before coalescence. The shape change of lower bubble

undergoes three processes: under the combined action of inertial force and buoyancy, it forms an ellipsoidal shape with E<1; Under the suction effect of upper bubble, the shape of lower bubble changes from an ellipsoid to a circle, with E=1; The influence of upper bubble on lower bubble deepens, and the shape changes from circular to long and narrow, extending along the y-axis to pear shaped, so E>1. As the lower bubble gets closer to upper bubble, the aspect ratio of lower bubble begins to decrease due to the surface tension of upper bubble and the extrusion of top fluid, but it is greater than 1. The aspect ratio of upper bubble is always less than 1, and the shape changes from round to ellipsoid, and finally gradually becomes flat. Due to the influence of surface tension of lower bubble, the bottom of upper bubble is sunken, and the aspect ratio continues to decrease until the two bubbles merge into a large bubble.

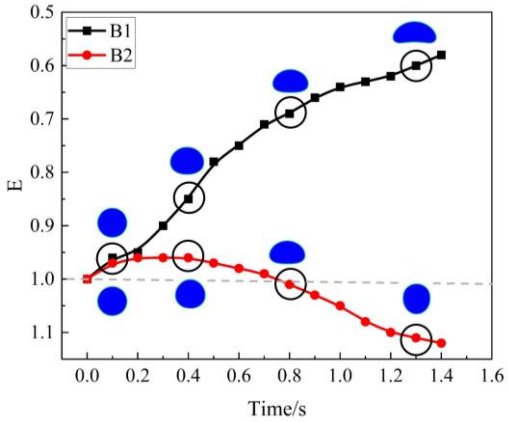

Fig. 10 The shape change of B1 and B2 before coalescence (s=2d)

3.3 Formation and Evolution of the Wake

Fig.11 shows the Ω diagram of coaxial double bubbles with d=2mm at different initial spacings when they begin to rise for 0.05 s (the initial stage of rise). From Fig. 11 (a), it can be seen that when s = 0.5d, the wake display of the upper and lower bubbles is connected, indicating that the lower bubble has entered the wake area of the upper bubble at 0.05s. The red area symbolizing the high intensity of vortex rotation ($\Omega \geq 0.95$ in this area, where the vorticity in the fluid rotation part is large and close to the rigid body rotation) accounts for a larger proportion, indicating that the lower bubble is more significantly sucked by the wake of the upper bubble.

From Fig. 11 (b) to (d), it can be seen that within the initial spacing range of d~2d, the wake of the double bubbles is still connected, indicating that lower bubble has entered the influence range of the wake of upper bubble, but the proportion of areas with high vorticity rotation (red area in the figure) decreases, and the shear part of the fluid vorticity increases, but the proportion of rotational vorticity is still large. As the initial spacing increases, the wake of the upper bubble can still affect the rise of the lower bubble, but the suction effect weakens and the acceleration effect obtained by the lower bubble decreases.

As shown in Fig. 11 (e), the lower bubble enters the end of upper bubble wake. At this moment, the lower bubble is less affected by the upper bubble wake than the initial spacing s of 0.5d, d, 1.5d, and 2d. In addition, the distribution and intensity of the rotation center of the wake around lower bubble remain basically unchanged, while the rotation intensity of the wake on

both sides of upper bubble increases. This is because the influence of the wake of upper bubble on lower bubble is reduced.

As shown in Fig. 11 (f), when the initial spacing increases to 4*d*, the lower bubble has not yet entered the wake influence range of the upper bubble at 0.05s, and the wake distribution around the two bubbles exists independently. The wake structure around the upper bubble is large but with low rotation intensity, while the wake size of the lower bubble is small but with high rotation intensity.

According to the setting of the simulation, the initial position of the lower bubble is fixed, and the setting of different spacing by adjusting the initial position of the upper bubble. According to the distribution of the wake structure of upper bubble in Fig. 11, the farther the upper bubble from the bottom of container, the larger the wake structure, and the greater the rotation intensity of the wake around bubble.

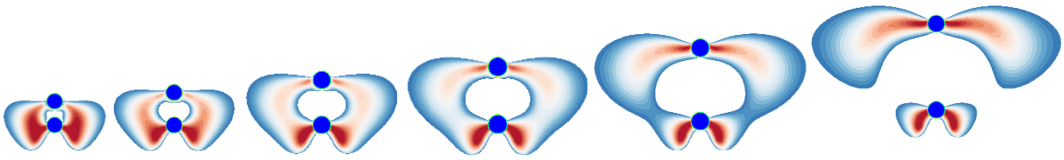

(a) *s*=0.5*d* (b) *s*=1*d* (c) *s*=1.5*d* (d) *s*=2*d* (e) *s*=3*d* (f) *s*=4*d*

Fig.11 Wake distribution of bubbles with different spacing at 0.05s

According to Fig. 11, the wake of the two bubbles with an initial spacing of 4d is independent of each other in the initial stage. Therefore, the *Ω* diagram of the wake evolution before the coalescence of double bubbles with an initial spacing of 4*d* is drawn to understand the wake change process before the coalescence of double bubbles, as shown in Fig.12. Fig.11 (f) shows that the wakes of the two bubbles are independent of each other at 0.05s. From Fig. 12 (a), it can be seen that at 0.1s, the lower bubble enters the end of the wake of upper bubble. At this time, the influence of the wake of the upper bubble on the behavior of the lower bubble is just beginning. There are obvious vortices on both sides of the wall and at the corners of the model because the bubble moves in glycerol and has wall adhesion. As time goes on, the distance between two bubbles gradually decreases, and the rotation intensity on both sides of lower bubble increases. As shown in Fig.12 (b), the fluid rotation center on both sides of upper bubble moves downward. Fig. 12 (c) shows that the vortex core separation occurs at 1.4 s, and the wake rotation center of the upper and lower bubbles keeps approaching. Finally, at 1.55 s, the wake center of the upper and lower bubbles becomes a whole cycle (Fig. 11 (e)). At this time, the upper bubble wake has the greatest suction effect on lower bubble, and the rising speed and shape of lower bubble change sharply.

Fig. 12 (f) and (g) show that the vortex core in the wake connection area of two bubbles is about to undergo separation and complete separation, which is different from the vortex core detachment at 1.4 seconds. After the vortex core detachment, it does not converge with the small vortex at the bottom but approaches the wall direction and enters the outer circulation area of the wake connection area of two bubbles. As shown in Fig. 12 (h), due to the secondary separation of the vortex core at 1.75 s, the vortex rotation area in the wake main connection area adjacent to the bubbles is reduced, and the suction effect of the upper bubble wake is reduced. The fluid squeezing between the two bubbles is obvious, and the resistance of lower bubble rising is increased. At this time, the lower bubble performs accelerated motion with reduced

acceleration. Figure 12 (i) shows the wake when the two bubbles completely coalesce into a large bubble at 2.0 s, and the rotation on both sides of the large bubble is lower than the rotation near the wall behind it.

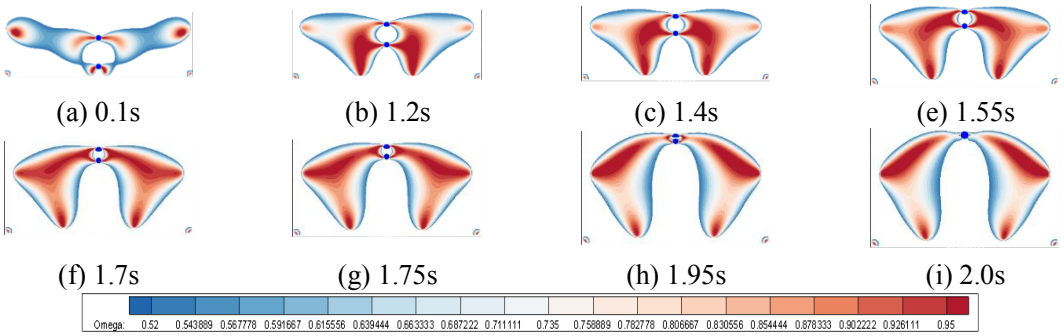

Fig.12 Wake evolution of two bubbles with initial spacing of 4*d*

4.Conclusion

In this paper, the gas-liquid two-phase flow characteristics of coaxial double bubbles rising process are studied by using numerical simulation. The main contributions are as follows: The velocity and deformation characteristics of the coaxial double bubbles during the rising process were explored. Based on the Q criterion, the flow field was identified and reconstructed by using vortex identification, and the formation, evolution, intensity, and morphological characteristics of the bubble wake were obtained. This study more comprehensively reflected the motion characteristics and wake characteristics of the coaxial double bubbles rising process, providing more theoretical basis for studying the multiphase flow in the bottom-blown molten pool. The main conclusions are as follows:

Motion behavior：The acceleration of coaxial double bubbles in the rising process is much larger than that of single bubble. The larger the initial distance and bubble diameter, the greater the difference of acceleration between coaxial double bubbles and single bubble. At the beginning, the upper bubble flattens from a circle, and as the two bubbles approach, the lower boundary of the upper bubble gradually depresses, and the aspect ratio is always less than 1. The shape of lower bubble is elongated in the vertical direction by the influence of upper bubble, changing from a circular shape to a pear shape. The minimum E is 0.85, the maximum can reach 1.2.

Wake characteristics：The wake of upper bubble moves down continuously during the rising process and is gradually connected with the wake of lower bubble. When the rotation center of the upper and lower bubbles is connected, the wake becomes a whole circulating flow. At this moment, the instantaneous acceleration of lower bubble is the largest, and the wake attraction effect is the strongest.

Acknowledgements

The authors appreciate the advising of Assoc. Prof. X. H. Zhang (State Key Laboratory of Complex Nonferrous Metal Resources Clean Utilization, Kunming University of Science and Technology). Thanks to the State Key Laboratory for the Clean Utilization of complex non-ferrous metal Resources.

Nomenclature

u	Velocity of the fluid (m/s)	T	Temperature (k)
p	Pressure (Pa)	Ω	Lagrange multiplier
ρ	Density (kg/m^3)	η	Viscosity (Pa×s)
σ	Surface tension coefficient (N/m)	d	Diameter (m)
t	Time(s)	L	Relative distance (m)

References

[1] Yang, K., et al., Identifying flow patterns in a narrow channel via feature extraction of conductivity measurements with a support vector machine, *Int. J., Sensors., 23 (2023),* pp.1907.

[2] Wang, S., et al., Bubble dynamics and its applications, Int. J., Journal of Hydrodynamics, *30(2018)*, pp:975-991.

[3] Miksis, M, J., et al., Rising bubbles, *Int. J., Journal of Fluid Mechanics., 123(1982),* 31-41.

[4] Amirnia, S., et al., Continuous rise velocity of air bubbles in non-Newtonian biopolymer solutions, *Int. J., Chemical Engineering Science., 94(2013),* pp.60-68.

[5] Zhang, L., et al., Chaotic characterization of macromixing effect in a gas–liquid stirring system using modified 0–1 test, *Int. J., Can J Chem Eng., 100(2022),* pp.261– 275.

[6] Raymond, F., et al., A numerical and experimental study of the terminal velocity and shape of bubbles in viscous liquids, *Int. J., Chemical Engineering Science., 55(2000),* pp.943-955.

[7] Hu, B., et al., Numerical study on the influence of liquid viscosity ratio on the hydrodynamics of a single bubble in shear-thinning liquid, *Int. J., Applied Mathematical Modelling., 103(2022),* pp. 122-140.

[8] Gao, D., et al., Study of bubble behavior in high-viscosity liquid in a pseudo-2D column using high-speed imaging, *Int. J., Chemical Engineering Science., 252 (2022),* pp. 117532.

[9] Mirsandi, H., et al., Numerical study on the interaction of two bubbles rising side-by-side in viscous liquids, *Int. J., Chemical Engineering Journal., 410 (2020),* pp.128257.

[10] Dekée, D., et al., Bubble velocity and coalescence in viscoelastic liquids, *Int. J., Chemical Engineering Science., 41(1986),* pp.2273-2283.

[11] Liu, J., et al., Numerical simulation of the interactions between three equal-interval parallel bubbles rising in non-Newtonian fluids, *Int. J., Chemical Engineering Science., 93 (2013),* pp. 55-66.

[12] Kong, G., et al., Hydrodynamic interaction of bubbles rising side-by-side in viscous liquids, *Int. J., Experiments in Fluids., 60 (2019),* pp. 155.

[13] Ramírez-Muñoz, J., et al., Drag force on interacting spherical bubbles rising in-line at large Reynolds number, *Int. J., International Journal of Multiphase Flow., 37 (2011),* pp.983-986.

[14] Feng, J., et al., Behaviour and dynamics of two bubbles in conjunct condition in high-viscosity liquids, *Int. J., Canadian Journal of Chemical Engineering., 94 (2016),* pp. 1583-1591.

[15] Tian, Z., et al., Interaction of two in-line bubbles of equal size rising in viscous liquid, *Int. J., Chinese Journal of Chemical Engineering., 28 (2020),* pp.54-62.

[16] Vahabi, M., et al., Interaction of a pair of in-line bubbles ascending in an Oldroyd-B liquid: A numerical study, *Int. J., European Journal of Mechanics - B/Fluids., 85 (2021),* pp. 413-429.

[17] Narayanan, S., et al., Coalescence of two bubbles rising in line at low reynolds numbers, *Int. J., Chemical Engineering Science., 29 (1974),* pp. 2071-2082.

[18] Li, M., et al., Experimental investigation of the behaviors of highly deformed bubbles produced by coaxial

coalescence, *Int. J., Experimental Thermal and Fluid Science, 117 (2020),* pp. 110114.

[19] Komasawa, I., et al., Wake behavior and its effect on interaction between spherical-cap bubbles, *Int. J., Journal of Chemical Engineering of Japan., 13(1980),* pp.103-109.

[20] Cano-Lozano, J., et al., Wake instability of a fixed axisymmetric bubble of realistic shape, *Int. J., International Journal of Multiphase Flow, 51 (2013),* pp. 11-21.

[21] Cano-Lozano, J., et al., Paths and wakes of deformable nearly spheroidal rising bubbles close to the transition to path instability *Int. J., Physical Review Fluids., 1(2016),* pp. 053604.

[22] Zhang, J., et al., What happens to the vortex structures when the rising bubble transits from zigzag to spiral, *Int. J., Journal of Fluid Mechanics., 828(2017),* pp.353-373.

[23] Sanada, T., et al., Motion and coalescence of a pair of bubbles rising side by side, *Int. J., Chemical Engineering Science., 64(2009),* pp. 2659-2671.

[24] Chai, X., et al., Wake acceleration effect on spherical bubbles aligned in-line, *Int. J., Progress in Nuclear Energy., 80(2015),* pp.74-79.

[25] Yan, H., et al., A single bubble rising in the vicinity of a vertical wall: A numerical study based on volume of fluid method, *Int. J., Ocean Engineering., 263(2022),* pp.112379.

[26] Amirnia, S., et al., Continuous rise velocity of air bubbles in non-Newtonian biopolymer solutions, *Int. J., Chemical Engineering Science., 94(2013),* pp.60-68.

[27] Liu, Z., et al., Study of bubble induced flow structure using PIV, *Int. J., Chemical Engineering Science., 60(2005),* pp.3537-3552.

[28] Hunt, J., et al., Eddies, streams, and convergence zones in turbulent flows, *Int. J., Studying Turbulence Using Numerical Simulation Databases-I1., 1988,* pp.193.

[29] Kong, G., et al. Oscillation dynamics of a bubble rising in viscous liquid, *Int. J., Experiments in Fluids., 60(2019),* pp.130.

[30] Liu, C., et al. New omega vortex identification method, *Int. J., Science China (Physics,Mechanics & Astronomy)., 59(2016),* pp.62-70.

· Paper submitted: 08 December 2023
· Paper revised: 08 January 2024
· Paper accepted: 11 January 2024